N89-17315

TURBINE AIRFOIL FILM COOLING*

L.D. Hylton, V. Nirmalan, B.K. Sultanian, and R.M. Kaufman
Allison Gas Turbine Division
General Motors Corporation
Indianapolis, Indiana

A combined analytical and experimental program is being conducted to develop an improved analytical approach, based on boundary layer theory, for predicting heat transfer to film cooled turbine airfoils. Extensive hot cascade tests have been performed at simulated engine conditions to provide film cooled airfoil heat transfer data to guide and verify development of new analytical tools. The results of the experimental phase of the program indicate that the film cooling process is a complex function of the thermal dilution and turbulence augmentation parameters with trends actually reversing as blowing strength and coolant-to-gas temperature ratio are varied. Some combinations of these parameters can actually result in increased heat transfer on portions of the airfoil. The pressure surface of the airfoil is shown to exhibit a considerably higher degree of sensitivity to changes in the film cooling parameters and, consequently, may prove to be more of a challenge than the suction surface in accurately predicting heat transfer levels with downstream film cooling.

INTRODUCTION

Emphasis is continuing to be placed on developing more accurate analytical models for predicting turbine airfoil external heat transfer rates. Performance goals of new engines require highly refined, accurate design tools to meet durability requirements. In order to obtain improvements in analytical capabilities, programs which focus on enhancing analytical techniques through verification of new models by comparison with relevant experimental data are required. The objectives of the current program are to develop an analytical approach, based on boundary layer theory, for predicting the effects of airfoil film cooling on downstream heat transfer rates and to verify the resulting analytical method by comparison of predictions with hot cascade data obtained under this program.

The overall approach to attaining the stated objective has involved a series of three programs. The initial program, performed under Contract NAS3-22761, assessed the capability of available modeling techniques to predict non-film cooled airfoil surface heat transfer distributions, acquired experimental data as needed for model verification, and provided verified improvements in the analytical models. This effort resulted in a baseline predictive capability and was reported in CR 168015 (ref. 1) published in May, 1983.

The problem of heat transfer predictions with film cooling was broken into sequential efforts with the effect of leading edge showerhead film cooling being investigated first, followed by a program to study the effects of the addition of discrete site suction and pressure surface injection. The effort on showerhead film cooling was performed under Contract NAS3-23695 and was reported in CR 174827 (ref. 2) published in July, 1985. As part of that program, a five-row, simulated common plenum

* This work is being performed under Contract NAS3-24619.

showerhead geometry was tested to determine differences between film and non-film cooled heat transfer coefficient distributions downstream of a leading edge, multiple hole film cooling array. Building on non-film cooling modeling improvements incorporated in a modified version of the STAN5 boundary layer code developed under Contract NAS3-22761, a program was developed to analytically model and predict differences resulting from leading edge mass injection.

The current program, being performed under Contract NAS3-24619, is intended to extend the analytical code development to include discrete site pressure and suction surface injection, with and without leading edge blowing, and to obtain relevant hot cascade data to guide and verify the model improvements.

PROGRAM DESCRIPTION AND STATUS

The current program contains separate, but interrelated, analytical and experimental tasks. The analytical task consists of three phases. The first phase, design mode analysis, has been completed. This effort consisted of demonstrating the use of the proposed boundary layer method in a design system environment. This demonstration resulted in predictions of heat transfer distributions for the film cooled airfoil used in the hot cascade tests performed during this program. The second analytical phase, method characterization, compares the predictions from the design mode analysis with the experimental data and establishes the deficiencies in the proposed method, and identifies modeling improvements that must be made. This effort is currently underway. The final analytical phase, method refinement/verification, will begin upon the completion of the method characterization phase. It will utilize the knowledge gained from the first two phases to develop an improved design tool for film cooled turbine airfoils.

The experimental task, which has just been completed, was an extension of the experimental work performed in the previous contract which was reported in reference 2. The hot cascade tests utilized the same facility, cascade and experimental techniques used in the previous contract, with the instrumented airfoil in the cascade replaced with one containing suction surface and pressure surface film cooling arrays in addition to a leading edge showerhead film cooling array. A photograph of the airfoil that was tested is shown in figure 1.

The airfoil cooling design incorporated three separate film cooling supply plenums. One plenum supplied an array of leading edge showerhead film cooling holes. The geometry of this film cooling hole array was identical to that utilized in Contract NAS3-23695. Two additional coolant supply plenums were incorporated into the vane; one to supply an array of holes on the suction surface and the other to supply an array of holes on the pressure surface of the airfoil. The three separate plenums allowed independent control of the flow to each region of the airfoil.

The suction surface array contained two staggered rows of holes centered at 25.2% of the suction surface length from the leading edge. Similarly, the pressure surface contained two staggered rows of holes centered at 22.5% of the pressure surface length from the leading edge.

All three hole arrays contained 1.0 mm (0.039 inch) diameter holes. The hole spacing-to-diameter ratio was 7.5 in the leading edge array and 3.0 for the other two arrays. The row spacing-to-diameter ratio was 4.0 in all three regions. The injection angle in the leading edge was the same as in the previous contract where the holes were aligned normal to the surface in the chordwise direction and at a

45° angle in the spanwise direction. The suction surface holes were inclined at 35° to the surface in the chordwise direction while the pressure surface holes were at 20° in the chordwise direction. Holes in both downstream arrays were normal to the surface in the spanwise direction. Also shown in figure 1 is the thermal barrier cutout region. This cut thermally isolated the film cooling supply plenums from the downstream regions of the airfoil where heat transfer measurements were made, similar to the technique used in the previous contract. Prior to testing, a thin, 0.254 mm (0.010 inch), shim was welded across the thermal barrier gap on both the pressure and suction surfaces. This provided a smooth, continuous surface on the airfoil. The retaining bar shown in figure 1 ensures that the airfoil profile was properly maintained after the thermal barrier cut was made.

The test matrix for which experimental data were obtained provided aerothermodynamic simulation of typical engine operating conditions. The test matrix is illustrated in figure 2. Data were obtained at cascade exit Mach numbers, M_2, of 0.75 and 0.90 and at exit Reynolds numbers, Re_2, of 1.5×10^6, 2.0×10^6, and 2.5×10^6. Coolant-to-gas absolute temperature ratios, TR or T_c/T_g, were varied from 0.65 to 0.85. The film cooling pressure ratio, PR or P_c/P_t, (film cooling supply plenum pressure-to-inlet stagnation pressure), was varied from 1.02 to 1.65 with most data taken in the range from 1.02 to 1.10.

RESULTS AND DISCUSSION

The testing associated with the experimental task has been completed, as has much of the data analysis. Efforts are just beginning on comparison of the data with the analytical model predictions. Consequently, the discussion that follows will focus primarily on a review of the experimental data and the trends that have been identified.

Prior to obtaining film cooled heat transfer data, baseline data (i.e. without film cooling) were obtained at the four base flow conditions (see fig. 2) corresponding to an exit Mach number, M_2 (or Ma_2), of 0.9 and exit Reynolds number, Re_2, of 1.5×10^6, 2.0×10^6, and 2.5×10^6 and at an exit Mach number of 0.75 with a Reynolds number of 2.0×10^6. In all cases, the inlet total temperature was maintained at a nominal value of 700K (1260 R). Figure 3 shows the vane surface-to-gas absolute temperature ratio, T_w/T_g, at an exit Mach number and Reynolds number of 0.9 and 2.0×10^6 respectively. In figure 3, and also in figures 4 through 14, the vertical dashed lines mark the locations of the film cooling hole rows and the vertical solid lines mark the locations of the thermal barrier on the suction and pressure surfaces. The cyclic vane surface temperature fluctuations seen near the trailing edge in figure 3 are due to coolant air flowing through the internal cooling holes. This temperature distribution, in addition to the internal boundary conditions at the 10 radial cooling holes, was used to obtain the local heat transfer coefficients by the method described in reference 2. The normalized local vane heat transfer coefficients, h/h_0, for this flow condition are presented in figure 4. The fluctuations in the local heat transfer coefficients are, again, caused by the presence of the radial coolant paths in the vane. Also in figure 4, the results predicted for the same conditions using the Allison - STANCOOL code developed under the previous NASA contracts (ref. 1 and 2), are given. Here, the solid curve is the predicted results with a constant wall temperature boundary condition. This prediction was made as part of the design mode analytical effort. The dashed curve is the prediction made using the actual measured surface temperature boundary condition. Since an appreciable temperature gradient existed, it seemed appropriate to use the variable temperature boundary condition for the prediction. Figure 4 shows a very reasonable comparison between the experimental data and the prediction using the

actual measured surface temperature for the boundary condition. This comparison illustrates the significance of the actual wall temperature boundary condition on heat transfer predictions.

The film cooled data that will be presented here include (a) data with only the suction side and pressure side film cooling arrays active, (b) data with all three film cooling arrays active, and (c) data with constant downstream injection and variable leading edge injection. The film cooling supply plenum pressure-to-inlet stagnation pressure ratio (P_c/P_t) was kept at nominal values of 1.02, 1.05 and 1.10 in the cases presented. In figures 5 through 14, the subscript le, on P_c/P_t, refers to the leading edge film cooling array, and the subscript ds refers to the downstream film cooling arrays on the pressure and suction surfaces. All tests were run with equal supply pressure for the two downstream arrays. Film coolant-to-gas absolute temperature ratios (T_c/T_g) were kept at nominal values of 0.65 (MIN), 0.75 (MED), and 0.85 (MAX).

To present the effects of film cooling on vane surface heat transfer, the ratio of Stanton number with film cooling to Stanton number without film cooling was calculated. However, instead of simply presenting the Stanton number ratio of film cooled to non-film cooled (St_{FC}/St_{NFC}), an alternate "no difference" parameter referred to as Stanton number reduction (SNR) and defined as

$$SNR = 1 - (St_{FC}/ST_{NFC}) \quad (1)$$

is used. Also, if the non-film cooled data and the film cooled data were obtained at equivalent exit Reynolds number and exit Mach number, SNR would approximately be equal to

$$SNR = 1 - (h_{FC}/h_{NFC}) \quad (2)$$

Figures 5 through 10 show some of the effects on Stanton number reduction of the different film cooling parameters for constant Mach number and Reynolds number conditions.

Figures 5 and 6 show the effects of varying the blowing strength at two constant thermal dilution (T_c/T_g) levels with only the downstream film cooling arrays active. The base flow conditions are at an exit Mach number of 0.9 and an exit Reynolds number of 2.5×10^6. Figure 5 shows the effect of varying the blowing strength (P_c/P_t) at the lowest coolant-to-gas temperature ratio ($T_c/T_g = 0.65$). A positive SNR is seen on both surfaces at all three blowing strengths indicating a comparatively large decrease in heat transfer due to downstream film cooling. A pronounced variation in SNR due to different blowing strengths is seen on the pressure surface. Also, on the pressure surface, as the blowing strength is increased, the effect of film cooling is felt further downstream. On the other hand, on the suction surface, there is hardly any effect due to varying blowing strengths. This is due to the lower freestream pressure on the suction surface causing the film coolant flow on that surface to be choked at this range of pressure ratios. Figure 6 shows similar behavior at a higher T_c/T_g ratio of 0.85 (MAX) though, as expected, with lower values of SNR due to a lower level of thermal dilution (warmer air being injected). Also, on the pressure surface near the film cooling holes, higher blowing strengths tend to increase heat transfer (i.e. a decrease in SNR values) by increasing the turbulence level in the region. This phenomena is more pronounced at the higher coolant-to-gas temperature ratios. It should also be noted that for the higher blowing strengths SNR increases over the last 60 percent of the airfoil; whereas, for the lower blowing strengths, the SNR decreases. This is the result of

the interaction of the thermal dilution and turbulence augmentation effects.

Figures 7 and 8 show some of the above data with additional data plotted to illustrate the effects of the thermal dilution at the lowest and highest blowing strengths of P_c/P_t = 1.02 (fig. 7) and 1.10 (fig. 8). On the suction surface, in both cases, there is a very noticeable effect due to different thermal dilution levels. Conversely, on the pressure surface, at the lowest blowing strength, as shown in figure 7, only a small effect is noticed. However, as seen in figure 8, there is a larger effect on the pressure surface due to varying thermal dilution at a higher blowing strength of P_c/P_t = 1.10. Also in figure 8, at T_c/T_g = 0.85, SNR is negative on the pressure surface at surface distance less than 50%. As mentioned before, this increase in heat transfer is due to the high blowing strength causing a higher turbulence level in the vicinity of the film cooling holes.

Figure 9 shows the effects of both the downstream and the leading edge film cooling arrays being active with varying blowing strengths at the MIN level of thermal dilution at the same flow conditions. In comparison to figure 5, the trends and levels of SNR are very similar to the case with only the downstream film cooling holes being active, indicating a very small effect due to the leading edge film cooling. However, on the pressure surface just downstream of the film cooling holes, higher values of SNR are seen due to the leading edge film cooling holes being active.

Figure 10 presents SNR data for the case where downstream film cooling hole arrays are at a constant blowing strength of 1.10 while the leading edge film cooling blowing strength is varied from 1.00 (no leading edge blowing) to 1.10. These data are at the flow conditions corresponding to an exit Mach number of 0.75 and an exit Reynolds number of 2.0×10^6. On the pressure surface, SNR is increased by low leading edge blowing values ($P_{c,le}/P_t$ = 1.02). However, at higher leading edge blowing strengths, SNR values drop off and at $P_{c,le}/P_t$ = 1.10 the SNR is lower than without any leading edge blowing. This indicates that high leading edge blowing rates can actually increase heat transfer over the entire pressure surface of the airfoil due to increased turbulence levels. On the other hand, very little effect of leading edge film cooling is seen on the suction surface.

Figures 5 through 10 represent the trends seen due to the various film cooling parameters and are very representative of other similar data at different cascade operating conditions.

Figures 11 and 12 illustrate the effect of varying the exit Mach number from 0.75 to 0.9 while keeping other flow and film cooling conditions constant. In these two instances, the downstream film cooling hole arrays are at blowing strengths, P_c/P_t, of 1.05 and the coolant-to-gas temperature ratios (T_c/T_g) are at 0.65 (MIN) (fig. 11) and 0.85 (MAX) (fig. 12). Also as before, SNR values indicate the effect of film cooling versus non-film cooling at identical flow conditions: therefore, in these cases, due to comparison of data at two different flow conditions, the two baseline conditions are also given in the legend. Figures 11 and 12 show that there is no major effect on SNR due to variations in Mach number on either the suction or pressure surfaces at the lower coolant-to-gas temperature ratio. However, on the pressure surface at the higher coolant-to-gas temperature ratio, figure 12 shows that at the lower Mach number, the effect of film cooling is more beneficial than at the higher Mach number.

Figures 13 and 14 show the effects of three different exit Reynolds numbers of 1.5×10^6, 2.0×10^6, and 2.5×10^6 on downstream film cooling. As in the previous

two figures, the baseline conditions for each set of data are also given in the legend. Figure 13 presents data at the lower coolant-to-gas temperature ratio of 0.65 and coolant pressure ratio of 1.10. On the pressure side, SNR increases with increasing Reynolds number indicating that a more favorable effect of film cooling is attainable at higher Reynolds numbers. A similar effect is seen on the suction surface, except that at two higher Reynolds numbers ($Re_2 = 2.0x10^6$ and $2.5x10^6$) the variations due to different exit Reynolds number is not as pronounced. In figure 14, where the coolant-to-gas temperature ratio is about 0.85, the effect of Reynolds number variation is not as marked as in the case of the lower coolant-to-gas temperature ratio.

In conclusion, the experimental data that have been obtained in this program at simulated engine conditions give insight into the physical phenomena that occur on a film cooled airfoil, and should provide a relevant data base for verification of new design tools. The results of the experimental phase of this program indicate that the downstream film cooling process is a complex function of the thermal dilution and turbulence augmentation parameters with trends actually reversing as blowing strength and coolant-to-gas temperature ratio are varied. The pressure surface of the airfoil is shown to exhibit a considerably higher degree of sensitivity to changes in the film cooling parameters and, consequently, should prove to be more of a challenge than the suction surface in accurately predicting heat transfer levels with downstream film cooling.

REFERENCES

1. L. D. Hylton, M. S. Mihelc, E. R. Turner, D. A. Nealy, and R. E. York, "Analytical and Experimental Evaluation of the Heat Transfer Distribution over the Surfaces of Turbine Vanes", NASA CR-168015, May 1983.

2. E. R. Turner, M. D. Wilson, L. D. Hylton, and R. M. Kaufman, "Turbine Vane External Heat Transfer", Vol I, NASA CR-174827, July 1985.

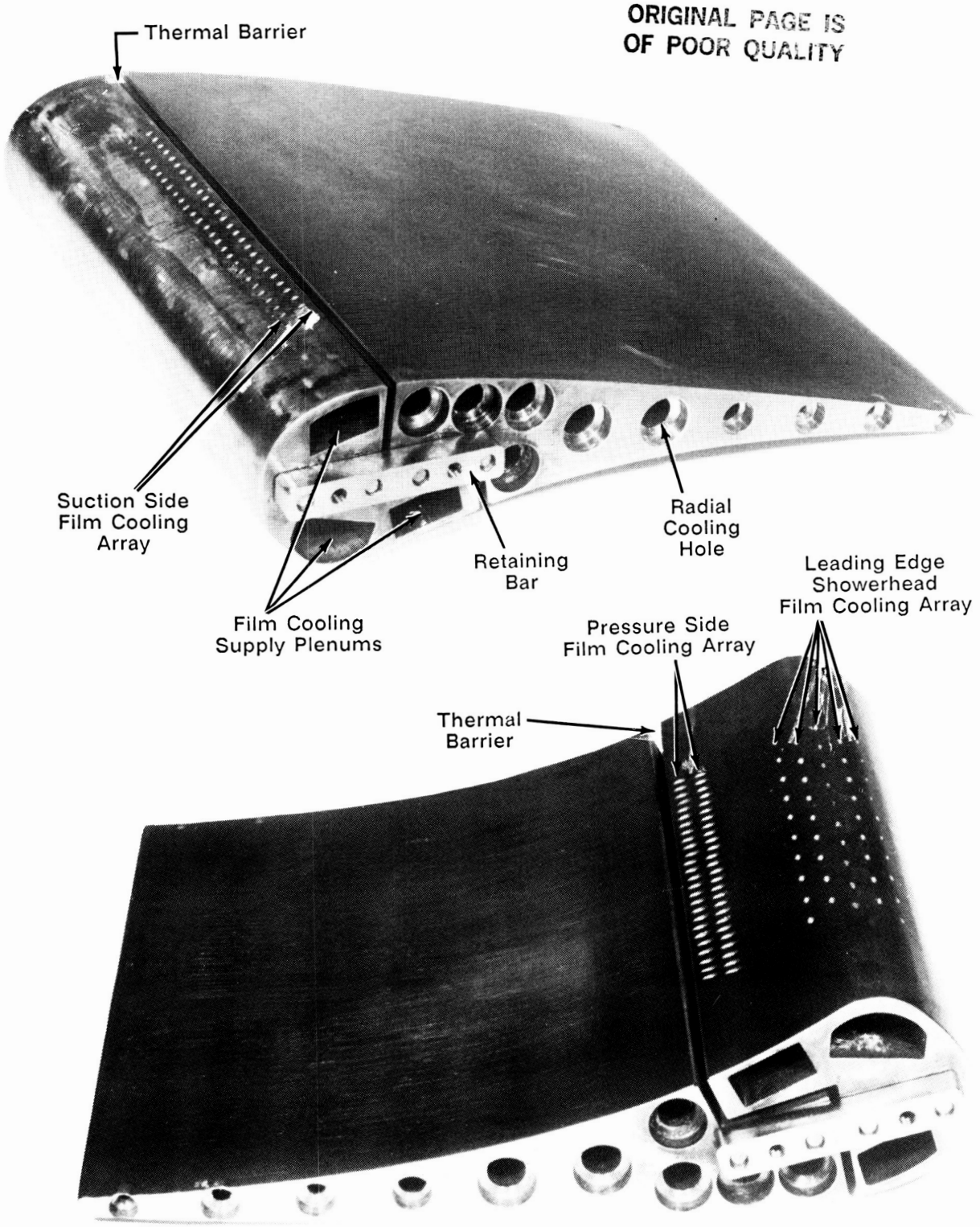

Figure 1. Film cooled airfoil for cascade tests

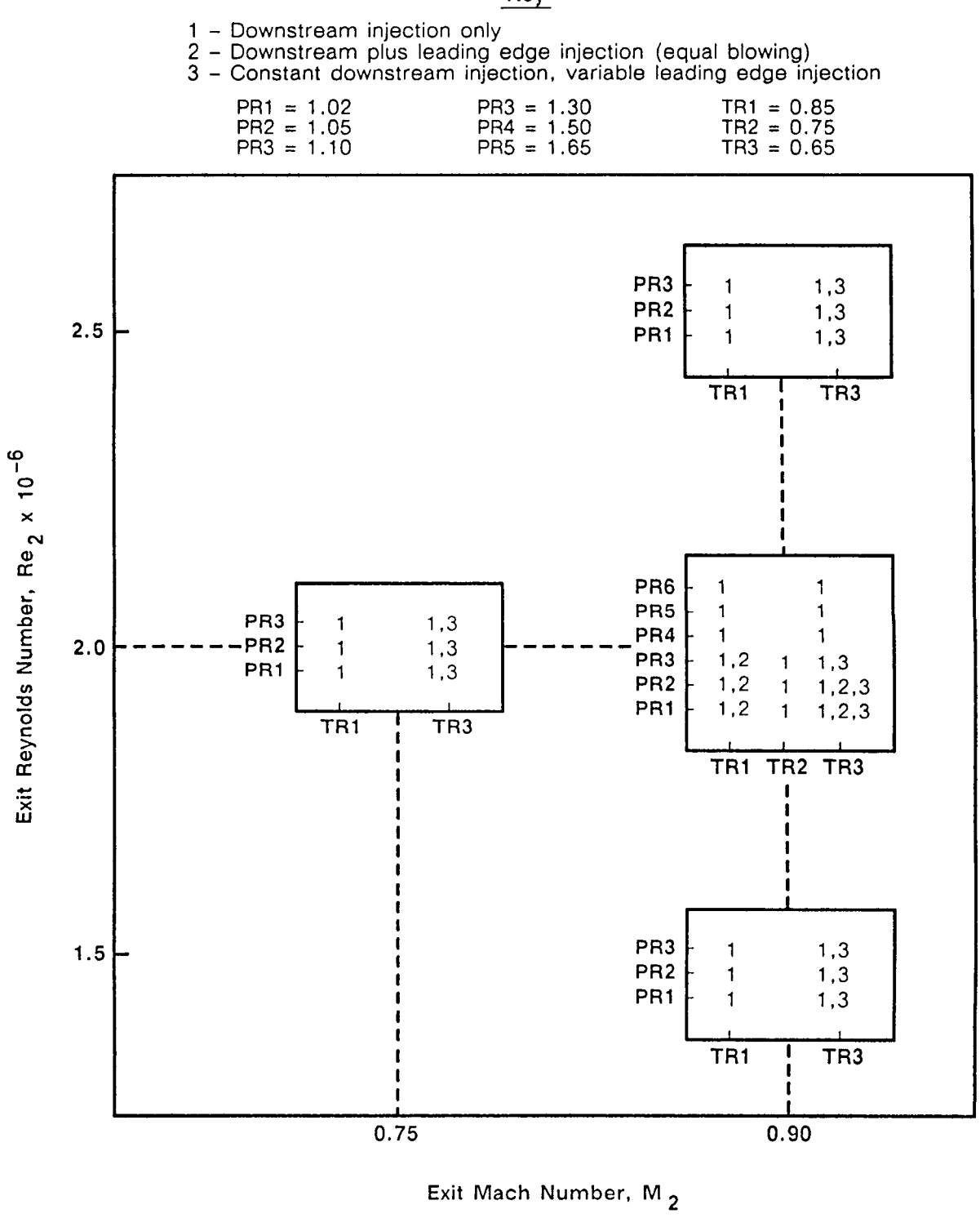

Figure 2. Test matrix

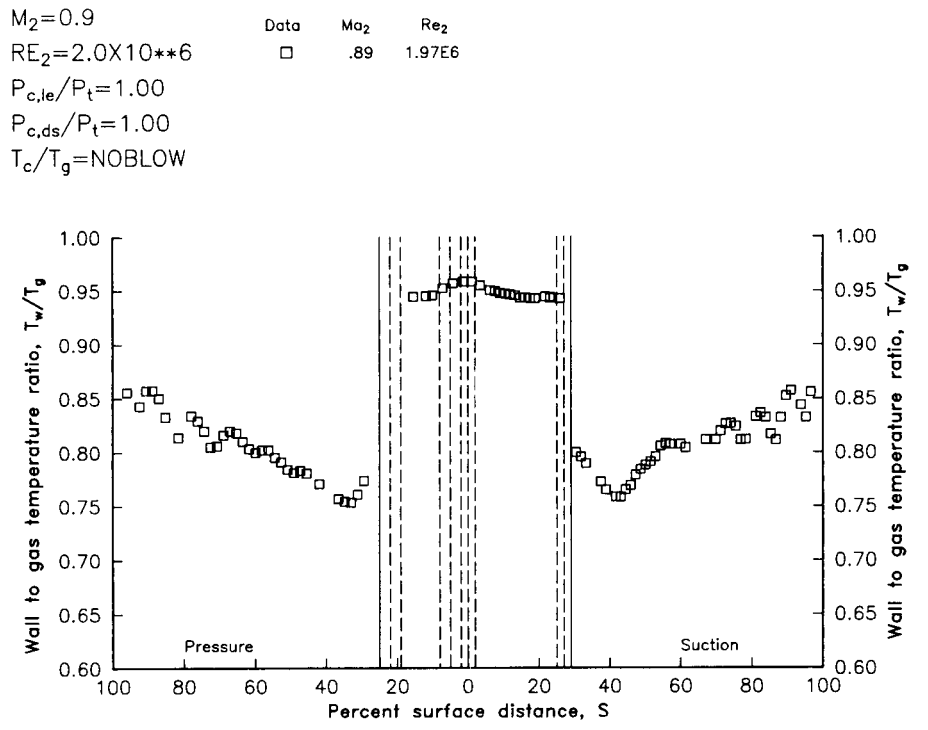

Figure 3. Vane surface-to-gas absolute temperature ratio distribution at baseline flow condition of Ma_2 = 0.9 and Re_2 = 2.0×10^6

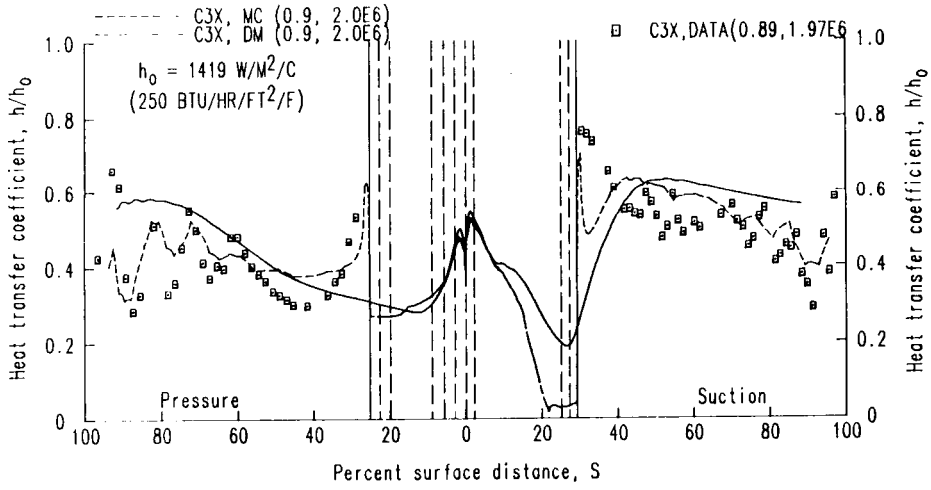

Figure 4. Vane surface local heat transfer coefficient distribution at baseline flow condition of Ma_2 = 0.9 and Re_2 = 2.0×10^6

M_2=0.9
RE_2=2.0X10**6
$P_{c,le}/P_t$=1.00
$P_{c,ds}/P_t$=VAR
T_c/T_g=MIN

Data	Ma_2	Re_2	$P_{c,ds}/P_t$	$P_{c,le}/P_t$	T_c/T_g
Base	.89	1.97E6			
△	.89	1.99E6	1.10	1.00	.68
◇	.90	2.00E6	1.05	1.00	.67
□	.90	1.99E6	1.02	1.00	.69

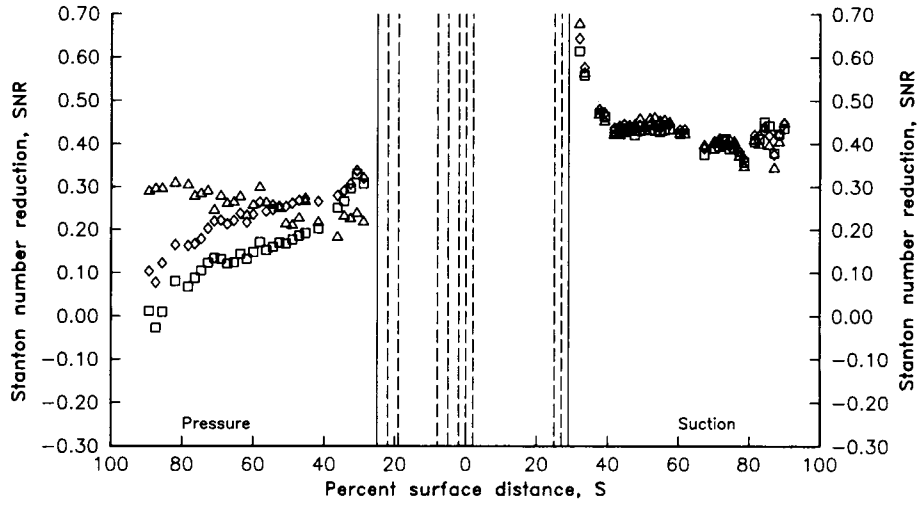

Figure 5. Effect of downstream blowing strength on heat transfer reduction (T_c/T_g = 0.65)

M_2=0.9
RE_2=2.0X10**6
$P_{c,le}/P_t$=1.00
$P_{c,ds}/P_t$=VAR
T_c/T_g=MAX

Data	Ma_2	Re_2	$P_{c,ds}/P_t$	$P_{c,le}/P_t$	T_c/T_g
Base	.89	1.97E6			
△	.90	2.03E6	1.11	1.00	.85
◇	.89	2.01E6	1.05	1.00	.86
□	.90	2.01E6	1.02	1.00	.84

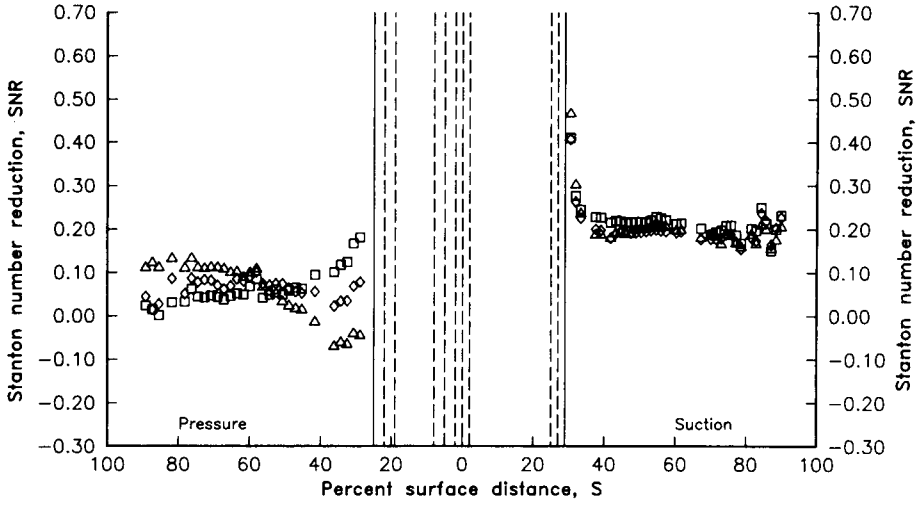

Figure 6. Effect of downstream blowing strength on heat transfer reduction (T_c/T_g = 0.85)

M_2=0.9
RE_2=2.0X10**6
$P_{c,le}/P_t$=1.00
$P_{c,ds}/P_t$=1.02
T_c/T_g=VAR

Data	Ma_2	Re_2	$P_{c,ds}/P_t$	$P_{c,le}/P_t$	T_c/T_g
Base	.89	1.97E6			
△	.90	2.01E6	1.02	1.00	.84
◇	.90	1.99E6	1.02	1.00	.75
□	.90	1.99E6	1.02	1.00	.69

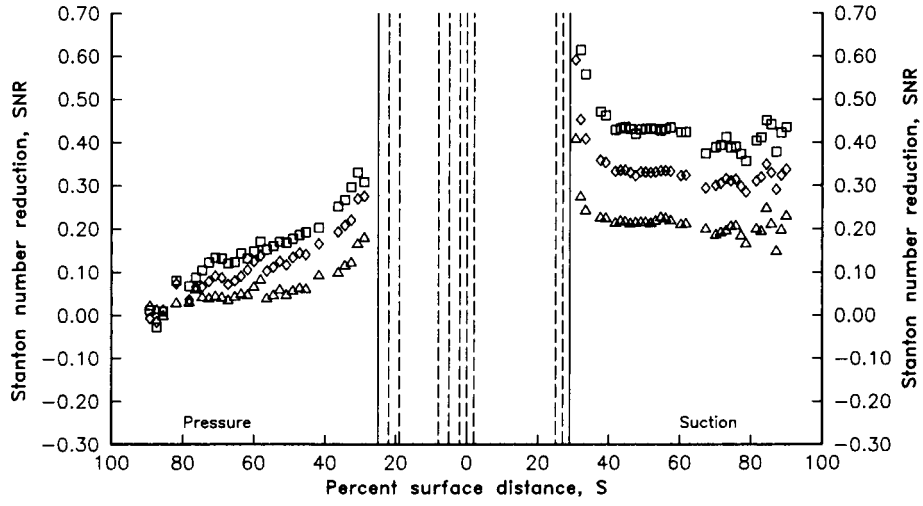

Figure 7. Effect of downstream film cooling thermal dilution on heat transfer reduction (P_c/P_t = 1.02)

M_2=0.9
RE_2=2.0X10**6
$P_{c,le}/P_t$=1.00
$P_{c,ds}/P_t$=1.10
T_c/T_g=VAR

Data	Ma_2	Re_2	$P_{c,ds}/P_t$	$P_{c,le}/P_t$	T_c/T_g
Base	.89	1.97E6			
△	.90	2.03E6	1.11	1.00	.85
◇	.90	2.01E6	1.11	1.00	.77
□	.89	1.99E6	1.10	1.00	.68

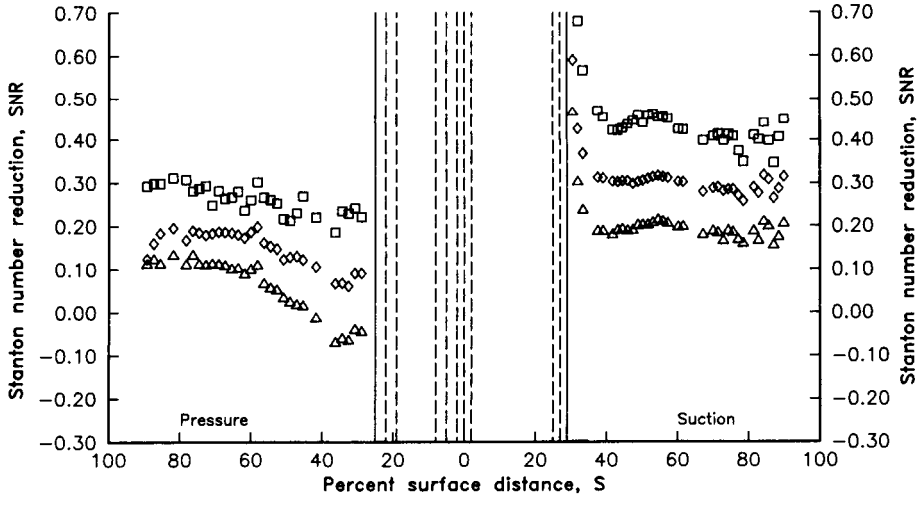

Figure 8. Effect of downstream film cooling thermal dilution on heat transfer reduction (P_c/P_t = 1.10)

M_2=0.9
RE_2=2.0X10**6
$P_{c,le}/P_t$=VAR
$P_{c,ds}/P_t$=VAR
T_c/T_g=MIN

Data	Ma_2	Re_2	$P_{c,ds}/P_t$	$P_{c,le}/P_t$	T_c/T_g
Base	.89	1.97E6			
△	.90	1.99E6	1.10	1.10	.66
◇	.90	2.03E6	1.05	1.05	.67
□	.92	2.04E6	1.02	1.02	.67

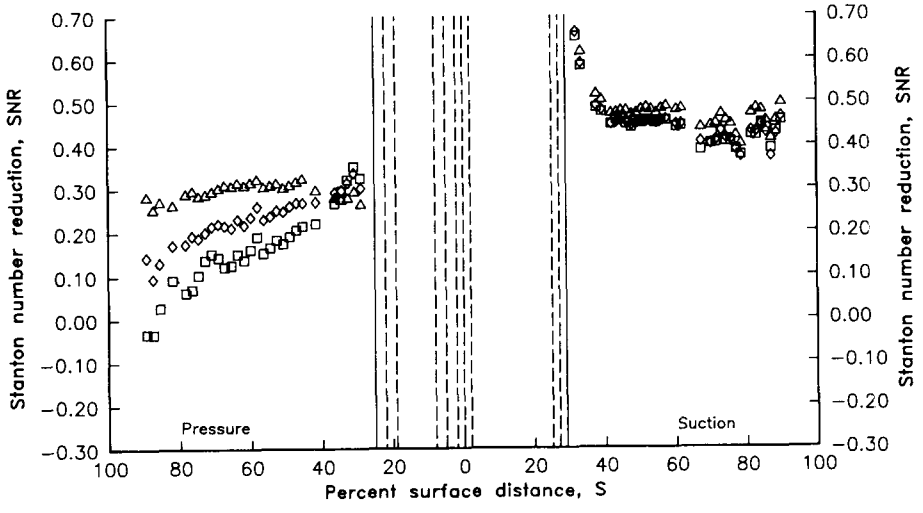

Figure 9. Effect of leading edge and downstream blowing strength on heat transfer reduction (T_c/T_g = 0.65)

M_2=0.75
RE_2=2.0X10**6
$P_{c,le}/P_t$=VAR
$P_{c,ds}/P_t$=1.10
T_c/T_g=MIN

Data	Ma_2	Re_2	$P_{c,ds}/P_t$	$P_{c,le}/P_t$	T_c/T_g
Base	.75	2.00E6			
○	.75	2.05E6	1.10	1.10	.67
△	.74	2.00E6	1.10	1.05	.65
◇	.75	2.01E6	1.10	1.02	.65
□	.75	2.00E6	1.10	1.00	.66

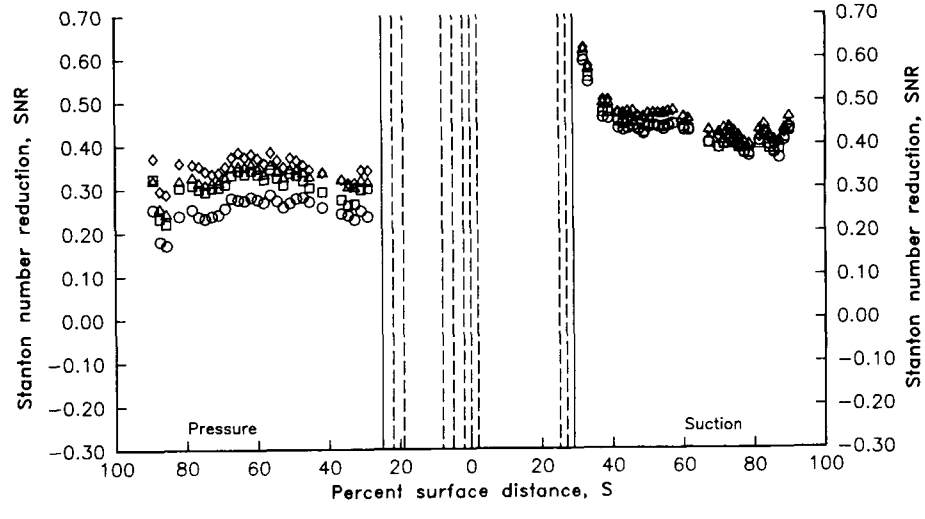

Figure 10. Effect of leading edge blowing strength with constant downstream blowing on heat transfer reduction (T_c/T_g = 0.65)

M_2=VAR
RE_2=2.0X10**6
$P_{c,le}/P_t$=1.00
$P_{c,ds}/P_t$=1.05
T_c/T_g=MIN

Data	Ma_2	Re_2	$P_{c,ds}/P_t$	$P_{c,le}/P_t$	T_c/T_g
Base	.75	2.00E6			
Base	.89	1.97E6			
◇	.75	2.00E6	1.05	1.00	.64
□	.90	2.00E6	1.05	1.00	.67

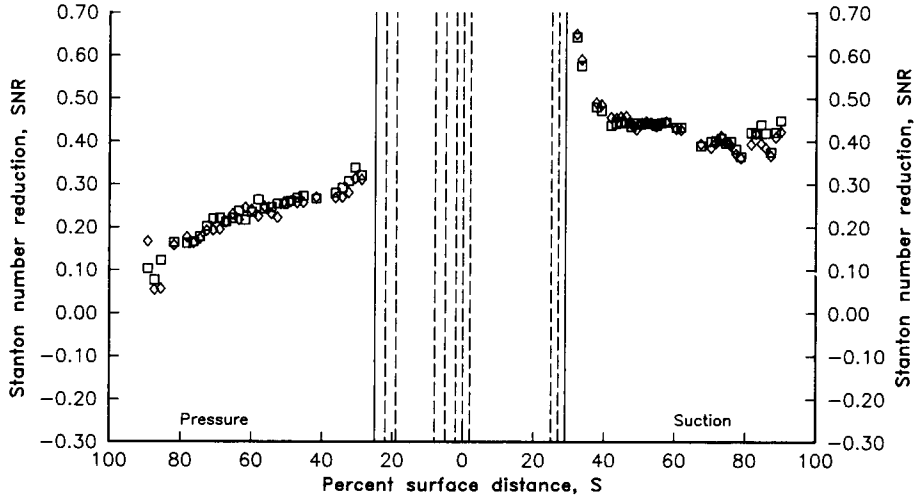

Figure 11. Effect of Mach number on heat transfer reduction (P_c/P_t = 1.05, T_c/T_g = 0.65)

M_2=VAR
RE_2=2.0X10**6
$P_{c,le}/P_t$=1.00
$P_{c,ds}/P_t$=1.05
T_c/T_g=MAX

Data	Ma_2	Re_2	$P_{c,ds}/P_t$	$P_{c,le}/P_t$	T_c/T_g
Base	.75	2.00E6			
Base	.89	1.97E6			
◇	.75	1.97E6	1.05	1.00	.86
□	.89	2.01E6	1.05	1.00	.86

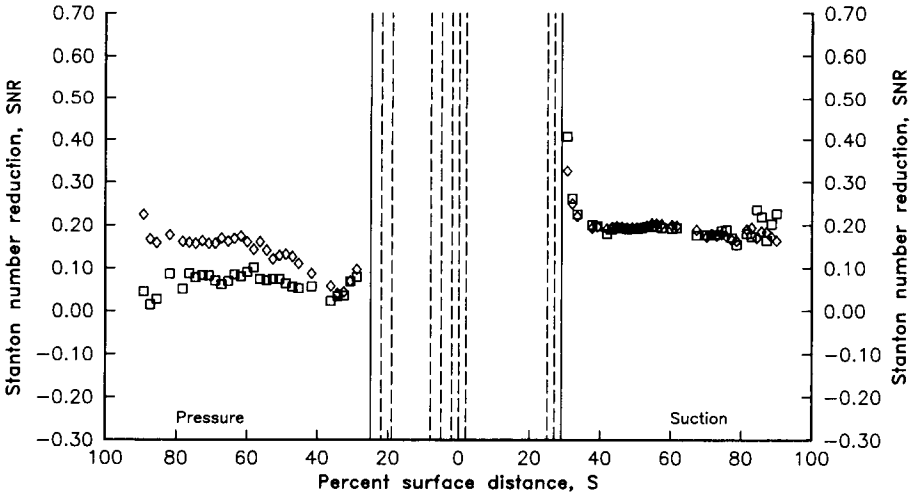

Figure 12. Effect of Mach number on heat transfer reduction (P_c/P_t = 1.05, T_c/T_g = 0.85)

M_2=0.9
RE_2=VAR
$P_{c,le}/P_t$=1.00
$P_{c,ds}/P_t$=1.10
T_c/T_g=MIN

Data	Ma_2	Re_2	$P_{c,ds}/P_t$	$P_{c,le}/P_t$	T_c/T_g
Base	.92	2.58E6			
Base	.89	1.97E6			
Base	.91	1.51E6			
△	.89	2.48E6	1.10	1.00	.66
◇	.89	1.99E6	1.10	1.00	.68
□	.89	1.55E6	1.10	1.00	.67

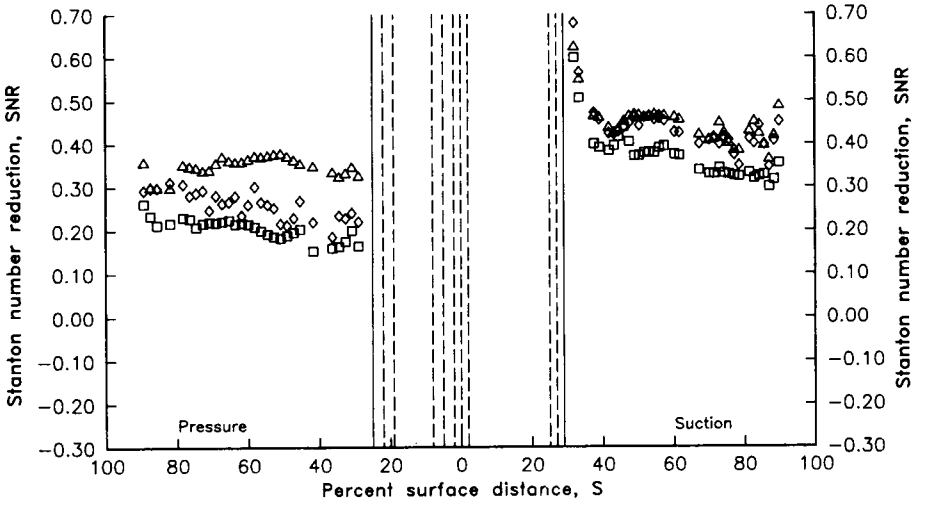

Figure 13. Effect of Reynolds number on heat transfer reduction (P_c/P_t = 1.10, T_c/T_g = 0.65)

M_2=0.9
RE_2=VAR
$P_{c,le}/P_t$=1.00
$P_{c,ds}/P_t$=1.10
T_c/T_g=MAX

Data	Ma_2	Re_2	$P_{c,ds}/P_t$	$P_{c,le}/P_t$	T_c/T_g
Base	.92	2.58E6			
Base	.89	1.97E6			
Base	.91	1.51E6			
△	.90	2.51E6	1.11	1.00	.86
◇	.90	2.03E6	1.11	1.00	.85
□	.90	1.52E6	1.11	1.00	.86

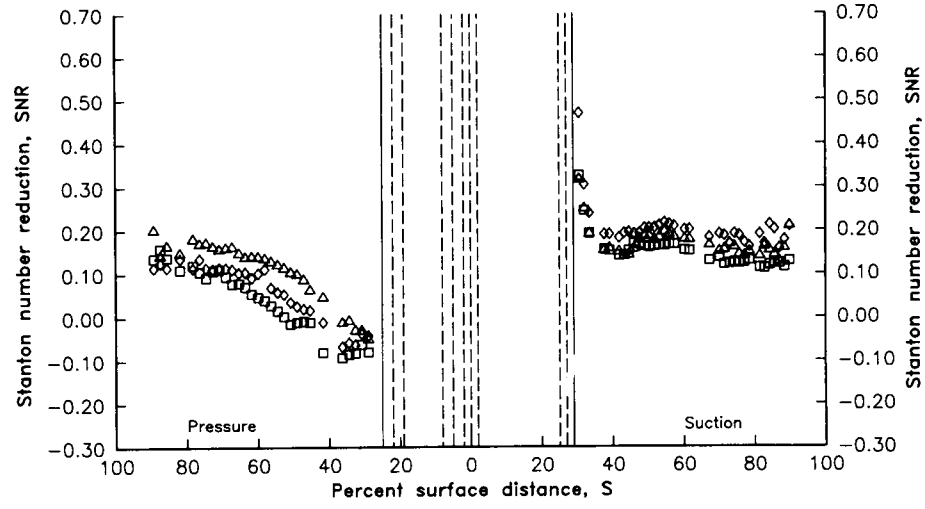

Figure 14. Effect of Reynolds number on heat transfer reduction (P_c/P_t = 1.10, T_c/T_g = 0.85)